

Production of bound $\mu^+\mu^-$ -systems in relativistic heavy ion collisions

I. F. Ginzburg^{1,2,*}, U. D. Jentschura^{3,†}, S. G. Karshenboim^{2,4,‡}, F. Krauss^{3,§},
V. G. Serbo^{2,5,**} and G. Soff^{3,††}

¹*Institute for Mathematics, 630090 Novosibirsk, Russia*

²*Max-Planck-Institut für Physik komplexer Systeme,
Bayreuther Straße 40, 01069 Dresden, Germany^{‡‡}*

³*Institut für Theoretische Physik, TU Dresden, 01062 Dresden, Germany*

⁴*D. I. Mendeleev Institute for Metrology, 198005 St. Petersburg, Russia*

⁵*Novosibirsk State University, 630090 Novosibirsk, Russia*

Abstract

Dimuonium (the bound system of two muons, $\mu^+\mu^-$ -atom) has not been observed yet. In this paper we discuss the electromagnetic production of dimuonium at RHIC and LHC in relativistic heavy ion collisions. The production of parastates is analyzed in the equivalent photon approximation. For the treatment of orthostates, we develop a three photon formalism. We determine the production rates at RHIC and LHC with an accuracy of a few percent and discuss problems related to the observation of dimuonium.

PACS numbers 25.75.-q, 25.75.Dw, 36.10.Dr

Typeset using REVTeX

*E-mail: ginzburg@math.nsc.ru

†E-mail: ulrich@theory.phy.tu-dresden.de

‡E-mail: sgk@onti.vniim.sbp.su

§E-mail: krauss@theory.phy.tu-dresden.de

**E-mail: serbo@math.nsc.ru

††E-mail: soff@physik.tu-dresden.de

‡‡temporary address

I. INTRODUCTION

The study of exotic electromagnetic bound systems and their properties is of theoretical and experimental interest. The bound $\mu^+\mu^-$ system (dimuonium, DM) has been subject to extensive theoretical investigations [1–5]. As demonstrated in [2], the decay rate of the dimuonic system is sensitive to radiative corrections from the so far unexplored time-like region of QED.

Although dimuonium has not been observed yet, a lot of different pathways for its production have been considered. For example, the production of dimuonium in the decay of the η -meson ($\eta \rightarrow \text{DM} + \gamma$) was investigated in Refs. [3,6], and in Ref. [4] the decay $K_L^0 \rightarrow \text{DM} + \gamma$ was considered. It has to be mentioned that in decays it is possible to produce only the $S = 1$ orthostates of dimuonium. Other calculations were performed for the production of dimuonium in collisions of charged particles (see Refs. [5,7]) and in collisions of photons with nuclei [5].

In this paper we investigate quite a different mechanism, which is based on the availability of relativistic heavy ions at high luminosities. Two new large hadron colliders, RHIC and LHC, are scheduled to be operative for the next decade. In Table I we list the decisive experimental parameters of the new colliders (see Refs. [8–10]). We consider here the purely electromagnetic production channel

$$A_1 A_2 \rightarrow A_1 A_2 + \text{DM},$$

where the A_i represent relativistic nuclei with nuclear charge numbers Z_i , and DM stands both for the $S = 0$ parastates of dimuonium (paradimuonium, PM) and for the $S = 1$ orthostates (orthodimuonium, OM). Because the nuclei do not change during the production process, they emit the photons *coherently*. This means that the perturbation parameter associated with each photon exchange between the nuclei and the produced system is not $\alpha \approx 1/137$, but rather $Z\alpha \sim 0.6$ (for Au and Pb). This leads to a very large flux of equivalent photons available for the production of exotic particles.

The C -even PM can be produced in collisions of an even number of virtual photons (two photon production mechanism, see the diagram of Fig. 1a). The C -odd orthostate (OM) can only be produced by an odd number of virtual photons, i.e. via bremsstrahlung production (one photon, Fig. 1b) and three photon production (see Fig. 1c). We consider here mainly the production of PM by two photons and the production of OM by three photons. Two photon and three photon fusion is the dominating process for the production of parastates and orthostates, respectively. The influence of multiphoton processes on the production rate is described by the effective perturbation parameter

$$\rho = \left(\frac{Z\alpha\Lambda}{m_{\mu\mu}} \right)^2 \lesssim 0.04, \quad (1)$$

with

$$1/\Lambda^2 = 1/6 \langle r^2 \rangle, \quad (2)$$

where $\langle r^2 \rangle$ is the mean square radius of the charge distribution of the nucleus, and the mass of the dimuonic atom is $m_{\mu\mu} \approx 2 m_\mu = 211$ MeV. Therefore, in all cases under consideration the multiphoton processes set limits on the accuracy on the level of 5%.

For our purpose it is sufficient to treat the dimuonia as compound neutral particles. To a good approximation their production rate then is proportional to the square of the wave function at the origin. In non-relativistic approximation it is only the probability density of S states at the origin which does not vanish,

$$|\psi_{nS}(0)|^2 = \frac{\alpha^3 m_\mu^3}{8\pi n^3}. \quad (3)$$

The production rate and the lifetime of the dimuonic atoms are both proportional to this value. The lifetimes of low lying states are of the order of $\tau \sim 10^{-12}$ s and are summarized in Table II. A brief discussion of the evaluation of the lifetime of parastates is given in Appendix A. Main decay channels are the annihilation processes

$$\text{PM} \rightarrow \gamma\gamma, \quad \text{OM} \rightarrow e^+e^-. \quad (4)$$

The rate of atomic transitions from excited S states to lower atomic states is of the same order of magnitude ($\alpha^5 m$) as the annihilation decay rate. It results in additional final states via atomic decays of excited DM levels which cascade through $S \rightarrow P \rightarrow S$ transitions. This leads to observable X-ray photons (at least two quanta) having ‘‘atomic’’ energy $\sim \alpha^2 m_\mu (n'^{-2} - n^{-2})/4$. Main properties of the various states can be found in Table II together with 2P paradimuonium which is produced in atomic transitions from 3S and 4S.

The detection of dimuonium would constitute a continuation of the recent investigations of exotic bound systems. Over the past years, experiments on antihydrogen [11,12], ponium [13] and the bound $\pi\mu$ system [14,15] have been reported.

This paper is organized as follows: first we investigate the production of paradimuonium in Sec. II. We then proceed to orthodimuonium, which is discussed in Sec. III. Finally we discuss the background in Sec. IV and summarize the results in Sec. V.

II. PARADIMUONIUM PRODUCTION

The production of an $S = 0$ parastate of dimuonium by a two photon process is represented by the diagram in Fig. 2. The diagram is evaluated using the equivalent photon approximation in the approach originally presented in Ref. [16]. Two nuclei A_1 and A_2 with identical charge number Z and atomic mass number A colliding with each other emit dn_i , ($i = 1, 2$) equivalent virtual photons within the energy ranges $(\omega_i, \omega_i + d\omega_i)$ and with four-momenta denoted as q_i . The virtualities of the photons are $Q_i^2 = -q_i^2$. Upon fusion, these photons produce a PM-bound state with four-momentum $p = q_1 + q_2$. Its mass squared $p^2 = W^2 = (q_1 + q_2)^2$ is approximately equal to $4m_\mu^2$. The most important contribution to the production process stems from photons with very small virtualities $Q_i^2 \ll m_\mu^2$. To a good approximation, the photons move in opposite directions, and we have $W^2 \approx 4\omega_1\omega_2$. In this very region the differential cross section $d\sigma$ for the $A_1 A_2 \rightarrow A_1 A_2 + \text{PM}$ process is related to the cross section $\sigma_{\gamma\gamma}$ for the process $\gamma\gamma \rightarrow \text{PM}$ by the equation

$$d\sigma_{\text{PM}} = dn_1 dn_2 \sigma_{\gamma\gamma}(W^2). \quad (5)$$

The spectrum of equivalent photons is given by Eq. (D.4) in Ref. [16], which upon omission of terms of order $\omega_i/E \ll 1$ reads

$$dn_i(\omega_i, Q_i^2) = \frac{Z^2 \alpha}{\pi} \frac{d\omega_i}{\omega_i} \left(1 - \frac{Q_{i \min}^2}{Q_i^2}\right) F^2(Q_i^2) \frac{dQ_i^2}{Q_i^2}, \quad Q_{i \min}^2 = \frac{\omega_i^2}{\gamma^2}. \quad (6)$$

In the calculations below we do not use the exact form factor of the nucleus $F(Q^2)$ but a simple approximation. This approximation corresponds to an exponentially decreasing charge distribution of the nucleus, whose mean square radius is adjusted to fit the experimental value (see Ref. [17], Eq. (B49)).

$$F(Q^2) = \frac{1}{1 + Q^2/\Lambda^2} \quad \text{where} \quad \Lambda^2 = \frac{0.164 \text{ GeV}^2}{A^{2/3}}. \quad (7)$$

According to Eq. (2), for Pb and Au the parameter $\Lambda \approx 70 \text{ MeV}$, and for Ca $\Lambda \approx 118 \text{ MeV}$. The approximate form factor enables us to perform some calculations analytically which else could only be done numerically.

It is useful to note that the integral over Q^2 converges fast at $Q^2 > \Lambda^2$. The decisive region of integration is given by the condition $Q_{\min}^2 \leq Q^2 \lesssim \Lambda^2$ (cf. Eq. (6)). Therefore the main contribution to the cross section is given by virtual photons with energies

$$\omega_i \lesssim \Lambda \gamma. \quad (8)$$

Because the two photon width of paradiuonium is small in comparison with its mass, we can use a δ -approximation for the cross section $\sigma_{\gamma\gamma}$ (for further details see Eq. (3.24) in Ref. [16] and Eq. (89.4) in Ref. [18]). For the 1^1S_0 para ground state, this approximation has the form

$$\sigma_{\gamma\gamma}(p^2) = 2 \pi^2 \alpha^5 \delta(p^2 - 4 m_\mu^2). \quad (9)$$

After the transformation

$$\begin{aligned} \frac{d\omega_1}{\omega_1} \frac{d\omega_2}{\omega_2} \delta(p^2 - 4 m_\mu^2) &= \frac{d\omega_1}{\omega_1} \frac{dp^2}{p^2} \delta(p^2 - 4 m_\mu^2) \\ &\rightarrow \frac{1}{4 m_\mu^2} \frac{d\omega_1}{\omega_1} \end{aligned} \quad (10)$$

we cast the cross section into the form

$$d\sigma_{\text{PM}} = \frac{\pi^2}{2} \alpha^5 \frac{d\omega_1}{\omega_1} \frac{dn_1(\omega_1, Q_1^2)}{d\omega_1} \frac{dn_2(\omega_2, Q_2^2)}{d\omega_2},$$

where $\omega_2 = m_\mu^2/\omega_1$. Using this formula, we derive the distribution of the produced PM atoms with respect to the energy ε and the transverse momentum p_\perp via the relations

$$\varepsilon = \omega_1 + \frac{m_\mu^2}{\omega_1}, \quad \mathbf{p}_\perp = \mathbf{q}_{1\perp} + \mathbf{q}_{2\perp}. \quad (11)$$

It is useful to note that the integral over Q^2 converges fast for $Q^2 > \Lambda^2$. Integrating $dn_i(\omega, Q_i^2)$ over Q_i^2 , we obtain the equivalent photon spectrum in dependence on the energy, $dn_i(\omega)$.

$$dn_i(\omega_i) = \frac{Z^2 \alpha}{\pi} f\left(\frac{\omega_i}{\Lambda \gamma}\right) \frac{d\omega_i}{\omega_i}. \quad (12)$$

The function

$$f(x) = (1 + 2x^2) \ln\left(\frac{1}{x^2} + 1\right) - 2 \quad (13)$$

drops very quickly at large x in accordance with Eq. (8) (indeed, $f(x) \leq 1/(6x^4)$ at $x \geq 1$). Finally, we obtain

$$\sigma_{\text{PM}} = \frac{Z^4 \alpha^7}{2 m_\mu^2} G(\delta), \quad \text{where} \quad \delta = \frac{m_\mu}{\Lambda\gamma} \quad (14)$$

and

$$\begin{aligned} G(\delta) &= \int_{\omega_{\min}}^{\omega_{\max}} \frac{d\omega_1}{\omega_1} f\left(\frac{\omega_1}{\Lambda\gamma}\right) f\left(\frac{\omega_2}{\Lambda\gamma}\right) \\ &= \int_{x_{\min}}^{x_{\max}} \frac{dx}{x} f(x\delta) f(\delta/x), \end{aligned} \quad (15)$$

with $x = \omega_1/m_\mu$. Because $\omega_i < E$ and $\omega_1\omega_2 = m_\mu^2$ we have $x_{\min} = m_\mu/E$ and $x_{\max} = E/m_\mu$. However, due to the fast decline of $f(x)$ at $x > 1$ we can expand these limits up to $x_{\min} = 0$ and $x_{\max} = \infty$ in very good approximation.

Numerical evaluation of the integral in Eq. (15) yields the following result for the total production cross sections

$$\sigma_{\text{PM}} = 10^{-30} \text{ cm}^2 \times \begin{cases} 0.15 & \text{for RHIC, Au mode,} \\ 1.35 & \text{for LHC, Pb mode,} \\ 0.0066 & \text{for LHC, Ca mode.} \end{cases} \quad (16)$$

The production cross sections for excited nS states are derived from the above cross section, which is obtained for the 1S states, with the aid of Eq. (3),

$$\sigma(nS) = \frac{\sigma(1S)}{n^3}. \quad (17)$$

The summation over n enhances the result of Eq. (16) by a factor of

$$\zeta(3) = \sum_{n=1}^{\infty} \frac{1}{n^3} \approx 1.202. \quad (18)$$

The distribution in energy for the paradimuonium atoms is given by the integrand of Eq. (15), using the relation Eq. (11). It is shown in Fig. 3.

We checked that the results depend only weakly on the choice of the form factor. With the help of a numerical computer program [19] we took into account the Gaussian form factor $\exp(-Q^2/\Lambda_g^2)$ with $\Lambda_g = 60 \text{ MeV}$ (for Pb and Au collisions) and $\Lambda_g = 100 \text{ MeV}$ (for Ca collisions) fixed on $\langle r^2 \rangle$. We found that this changes the final result presented in Eq. (16) by less than one percent. The effect of omitting terms of the order $\mathcal{O}(Q_i^2/m_\mu^2)$ in the equivalent photon spectrum Eq. (6) is also negligible. The relative contribution of the omitted terms is of the order of

$$\eta_2 = \frac{\Lambda^2}{2m_\mu^2 L}, \text{ and with } L = \ln \frac{1}{\delta^2} = \ln \frac{\Lambda^2 \gamma^2}{m_\mu^2} \text{ it follows } \eta_2 \sim (1 \div 2)\%. \quad (19)$$

The effect of processes involving more than two photons is governed by the parameter ρ from Eq. (1) and we recall that their effect is on the level of roughly 5 %.

It is instructive to consider additionally the leading logarithmic approximation (LLA) for the process. In the LLA, we approximate $f(x)$ by $2 \ln(1/x)$. The restriction $Q_{i \min}^2 \lesssim \Lambda^2$ corresponds to $m_\mu^2/(\Lambda\gamma) < \omega_1 < \Lambda\gamma$. Therefore

$$G^{\text{LLA}}(\delta) = \frac{2}{3}L^3, \quad (20)$$

and

$$\sigma_{\text{PM}}^{\text{LLA}} = \frac{Z^4 \alpha^7}{3 m_\mu^2} L^3. \quad (21)$$

The above result is in good agreement with the old result of [20] (see also Eq. (2.4) in review [16]). However, for the energies discussed in this paper the LLA does not provide sufficient precision. The ratio G^{LLA}/G is 1.5 for Pb at LHC and 2 for Au at RHIC. Hence, the LLA gives only a crude estimate for the energies discussed.

III. ORTHODIMUONIUM PRODUCTION

Orthodimuonium can be produced by bremsstrahlung (the relevant diagram is depicted in Fig. 1b) and by three photon fusion (see Fig. 1c). For production processes induced by relatively light particles (like e^+e^- or pp collisions) the three photon cross section $\sigma_{3\gamma}$ corresponding to Fig. 1c is suppressed by a factor α^2 compared to the cross section for bremsstrahlung production, σ_{br} . By contrast, for heavy ion collisions another parameter enters the calculation: the large nuclear mass M . Bremsstrahlung of heavy particles is suppressed by a factor $1/M^2$, so we obtain

$$\sigma_{\text{br}} \propto Z^6 \alpha^7 / M^2,$$

whereas for three photon production there is no such suppression,

$$\sigma_{3\gamma} \propto Z^6 \alpha^9 / m_\mu^2. \quad (22)$$

The ratio

$$\frac{\sigma_{\text{br}}}{\sigma_{3\gamma}} \lesssim \frac{1}{\alpha^2} \left(\frac{m_\mu}{M} \right)^2 = \begin{cases} 1/150 & \text{for RHIC, Au mode,} \\ 1/190 & \text{for LHC, Pb mode,} \\ 1/7 & \text{for LHC, Ca mode} \end{cases}$$

is small. Moreover, a more accurate estimate for CaCa collisions at LHC decreases this ratio at least by a factor of three. Therefore, the 3 photon production dominates in relativistic heavy ion collisions. In Fig. 1c only one representative diagram for three photon fusion is depicted. For a complete analysis, we need to take into account two classes of diagrams, in

which the single photon is emitted by either one of the nuclei (see Fig. 4a and Fig. 4b). The corresponding cross section, which is proportional to the square of the amplitude for the particular processes, is given by

$$d\sigma_{\text{OM}} = d\sigma_a + d\sigma_b + d\sigma_{\text{interf}} = 2 d\sigma_a \quad (23)$$

because the interference term $d\sigma_{\text{interf}}$ disappears after azimuthal averaging. Thus we may restrict ourselves to an analysis of the cross section for the process in Fig. 4a, denoted as $d\sigma_a$. To a very good approximation, this cross section can be expressed by the number of equivalent photons dn_1 emitted from one of the nuclei, given by Eq. (12), and the cross section for the process $\gamma A \rightarrow \text{OM} + A$, denoted as $\sigma_{\gamma A}$,

$$d\sigma_a = dn_1 \sigma_{\gamma A}. \quad (24)$$

We thereby assume that the incident photon in the process $\gamma A \rightarrow \text{OM} + A$ is a virtual photon in the framework of the equivalent photon approximation and thus exhibits a small virtuality $Q^2 \ll \Lambda^2 < 4m_\mu^2$. Therefore, we neglect the virtuality of this incident photon in the cross section $\sigma_{\gamma A}$. The subprocess $\gamma A \rightarrow \text{OM} + A$ is described by the set of diagrams of Fig. 5. We calculate its cross section $\sigma_{\gamma A}$ in the region of large energies and relatively small transverse momenta $|\mathbf{p}_\perp|$ of the produced OM. We have the kinematical conditions (the subscript 'th' denotes the threshold value)

$$s_\gamma = 2q_1 \cdot P_2 \gg s_{\text{th}} = 4m_\mu M \quad \text{and} \quad |\mathbf{p}_\perp| \lesssim m_\mu.$$

We note, that a loop integral has to be evaluated for this subprocess. Its contribution is rather different from what would be obtained within the standard equivalent photon distribution for the two remaining photons.

It is convenient to perform the calculations involved using the impact representation, which has been employed in QED and QCD for a number of processes with two photon or two gluon exchange (in the t -channel). More details on this approach are described in Refs. [21–24]. In this representation the amplitude $M_{\gamma A}$ which corresponds to the whole set of diagrams of Fig. 5 is written with an accuracy $\sim m_\mu^2/s_\gamma$ in the form of a two-dimensional integral over the transverse components of the momentum of the virtual photon,

$$M_{\gamma A} = i \int \frac{d^2\mathbf{k}_\perp}{(2\pi)^2} \frac{J_\gamma J_A}{\mathbf{k}_\perp^2 (\mathbf{p}_\perp - \mathbf{k}_\perp)^2}. \quad (25)$$

The impact factors J_γ and J_A correspond to the upper and lower block of the diagrams in Fig. 5. The diagrams in Fig. 5 are regarded as being cut by the photon lines of the lower block, dividing the process into two partial virtual processes, $\gamma + \gamma\gamma \rightarrow \text{OM}$ (upper block) and $A \rightarrow \gamma\gamma + A$ (lower block). The impact factor J_γ then corresponds to the virtual transition $\gamma + \gamma\gamma \rightarrow \text{OM}$, and J_A corresponds to the virtual transition in the lower block ($A \rightarrow \gamma\gamma + A$). The impact factor J_A for a charged point-like particle was found in [21,22] as $J_A = 4\pi\alpha Z^2$. In our case we should take into account the shape of the nucleus and modify this impact factor according to

$$J_A = 4\pi\alpha Z^2 F(\mathbf{k}_\perp^2) F((\mathbf{p}_\perp - \mathbf{k}_\perp)^2). \quad (26)$$

The impact factor J_γ for the virtual transition $\gamma + \gamma\gamma \rightarrow \text{OM}$ is similar to the impact factor for the virtual transition $\gamma + gg \rightarrow \Psi$ which was introduced for the description of the hard diffractive process $\gamma q \rightarrow \Psi q$ [24]. Adjusting for the different couplings and masses, we immediately obtain

$$J_\gamma = 4\pi \alpha^{9/2} \left[\frac{m_\mu^2}{m_\mu^2 + \mathbf{p}_{1\perp}^2} - \frac{m_\mu^2}{m_\mu^2 + (\mathbf{p}_{1\perp} - \mathbf{k}_\perp)^2} \right] \mathbf{e}_\gamma \mathbf{e}_{\text{OM}}^*. \quad (27)$$

Here $\mathbf{p}_{1\perp} = \mathbf{p}_{2\perp} = 1/2 \mathbf{p}_\perp$, and \mathbf{e}_γ and \mathbf{e}_{OM} are the polarization vectors for the initial photon and the final state OM. From Eq. (27) it follows that the helicity is conserved in the $\gamma \rightarrow \text{OM}$ transition. Therefore, the OM is transversely polarized and is produced in two polarization states only (not three states).

We finally obtain the cross section as

$$d\sigma_{\gamma A} = Z^4 \alpha^8 \left| \Phi(\mathbf{p}_\perp^2) \mathbf{e}_\gamma \mathbf{e}_{\text{OM}}^* \right|^2 \frac{d^2 \mathbf{p}_\perp}{m_\mu^4}, \quad (28)$$

where $\Phi(\mathbf{p}_\perp^2)$ is determined by an integral related to the amplitude $M_{\gamma A}$ given in Eq. (25). $\Phi(\mathbf{p}_\perp^2)$ can be written as

$$\Phi(\mathbf{p}_\perp^2) = \frac{1}{\pi} \int F \left(\frac{(\mathbf{r} + \mathbf{n})^2 \mathbf{p}_\perp^2}{4} \right) F \left(\frac{(\mathbf{r} - \mathbf{n})^2 \mathbf{p}_\perp^2}{4} \right) \frac{\mathbf{r}^2 - 1}{(\mathbf{r} - \mathbf{n})^2 (\mathbf{r} + \mathbf{n})^2} \frac{d^2 r}{(1 + \tau)(1 + \tau \mathbf{r}^2)} \quad (29)$$

where \mathbf{r} is a two-dimensional vector with no physical dimension, over which the integration has to be performed. \mathbf{n} is a unit vector defined by

$$\mathbf{n} = \frac{\mathbf{p}_\perp}{|\mathbf{p}_\perp|},$$

and τ is given by

$$\tau = \frac{\mathbf{p}_\perp^2}{4 m_\mu^2}.$$

After integrating over the azimuthal angle of OM, summing over the polarizations of the final state (OM spin states) and averaging over the polarizations of the initial state (photon polarizations), we obtain

$$\sigma_{\gamma A} = B \frac{\pi Z^4 \alpha^8}{m_\mu^2} \frac{\Lambda^2}{m_\mu^2} \quad (30)$$

where the dimensionless constant B follows from

$$B = \int_0^\infty (\Phi(\mathbf{p}_\perp^2))^2 \frac{dp_\perp^2}{\Lambda^2} = \int_0^\infty (\Phi(\Lambda^2 u))^2 du \quad (31)$$

and Λ is the form factor scale defined in Eq. (7).

The value of the constant B depends stronger on the shape of the form factor than the corresponding quantity for paradimuonium. We used a realistic form factor of the nuclear charge density $\rho(\mathbf{r})$ for which we employed the model [25]

$$F(\mathbf{k}^2) = \frac{1}{Ze} \int d^3r e^{i\mathbf{k}\cdot\mathbf{r}} \rho(\mathbf{r}),$$

with

$$\rho(\mathbf{r}) = \frac{Ze}{N} \frac{1}{1 + \exp((r - R)/a)}. \quad (32)$$

The parameters are

$$R = 1.18 A^{1/3} \text{ fm}, \quad a = 0.53 \text{ fm}.$$

N is the normalization factor chosen such that $\int d^3r \rho(\mathbf{r}) = 1$.

The evaluation of the constant B is performed numerically on IBM RISC/6000 workstations. Because the form factor Eq. (32) is a function of $\mathbf{k}^2 R^2$ with $R \propto \Lambda^{-1}$, the constant B has the same value for all nuclei considered in this paper. We obtain

$$B = 0.85. \quad (33)$$

It is useful to consider the sensitivity of the result on the choice of the form factor. With the approximate form factor given in Eq. (7) the function Φ is calculated in the Appendix B analytically (with an additional approximation $\tau = 0$ in the denominators of Eq. (29)). Further evaluation results in $B = 0.93$, this value is in fair agreement with the exact value from Eq. (33).

Because the cross section of the subprocess $\gamma A \rightarrow \text{OM} + A$ (cf. Eq. (30)) is energy independent in the discussed limit, the remaining integration of Eq. (24) is in fact an integration over the equivalent photon spectrum only. Let ω_2 be the total energy of both exchanged photons in Fig. 4. Then we have as in the previous section $4\omega_1\omega_2 = 4m_\mu^2$ (due to four-momentum conservation and the kinematics of the process) and $\omega_2 \lesssim \Lambda\gamma$ (due to the nuclear form factor). Thus a lower limit for ω_1 is

$$\omega_1 > \frac{m_\mu^2}{\omega_{2\text{max}}} \approx \frac{m_\mu^2}{\Lambda\gamma}. \quad (34)$$

The upper bound in this integration can be set to ∞ due to the fast decrease of the equivalent photon spectrum at large energy. We obtain (using the notation $\delta = m_\mu/(\Lambda\gamma)$ introduced previously)

$$\sigma_a = \frac{Z^2\alpha}{\pi} H(\delta) \sigma_{\gamma A}, \quad (35)$$

where

$$H(\delta) = \int_{m_\mu^2/(\Lambda\gamma)}^{\infty} \frac{d\omega_1}{\omega_1} f\left(\frac{\omega_1}{\Lambda\gamma}\right) = \int_{\delta^2}^{\infty} \frac{dx}{x} f(x) = \begin{cases} 57 & \text{for RHIC, Au mode,} \\ 202 & \text{for LHC, Pb mode,} \\ 247 & \text{for LHC, Ca mode.} \end{cases} \quad (36)$$

Finally, the cross section for the OM production is equal to (cf. Eqs. (22,23,30,35)),

$$\sigma_{\text{OM}} = 2 \frac{Z^6 \alpha^9}{m_\mu^2} \frac{\Lambda^2}{m_\mu^2} B H(\delta). \quad (37)$$

The numerical values are

$$\sigma_{\text{OM}} = 10^{-30} \text{ cm}^2 \times \begin{cases} 0.021 & \text{for RHIC, Au mode,} \\ 0.089 & \text{for LHC, Pb mode,} \\ 0.000069 & \text{for LHC, Ca mode.} \end{cases} \quad (38)$$

The ratio for the production cross section for the ortho and para states is given by

$$\frac{\sigma_{\text{OM}}}{\sigma_{\text{PM}}} = 4 \left(\frac{Z\alpha\Lambda}{m_\mu} \right)^2 B \frac{H(\delta)}{G(\delta)} = \begin{cases} 0.144 & \text{for RHIC, Au mode,} \\ 0.066 & \text{for LHC, Pb mode,} \\ 0.010 & \text{for LHC, Ca mode.} \end{cases} \quad (39)$$

Hence, we expect predominantly a production of para states in relativistic heavy ion collisions.

IV. ESTIMATE OF THE BACKGROUND

The dimuonic atoms are neutral systems produced by a number of photons which are approximately on-shell and collinear to the colliding ions. So the angular spread of the dimuonia with respect to the beam-axis is of the order of $\mathcal{O}(\gamma^{-1})$. The rapidity of the DM particles will be correspondingly high. Therefore the DM systems will not be observed directly by any detector with a low rapidity coverage.

The dominant decay channels of DM are $\gamma\gamma$ (for PM) and e^+e^- (for OM, cf. Eq. (4)). Dimuonium could be observed via detection of these decay products. We will investigate in this Section the influence of three sources of background on the prospective measurements,

- photon and electron-positron background originating from hadronic processes in the interaction region,
- free electron-positron pair production shadowing the signal from the decaying orthodimuonium and
- photon pair production by the two colliding nuclei shadowing the signal from the decaying paradimuonium.

The above sources of background are expected to affect mainly the signal of those dimuonium atoms which decay in or near the interaction region of the heavy ion collision.

First we consider photon and electron-positron background originating from inelastic hadronic processes in the interaction region. This background will affect the signal from both OM and PM atoms. In these inelastic processes, one or both of the nuclei dissolve to some extent. One can roughly divide these processes into two classes. The first are mainly hadronic processes, where the two nuclei collide and the strong interaction takes effect. The cross section for this class can be estimated as $\sigma_{AA} \approx 4 A^{2/3} \sigma_{pp}$, which for the nuclei under investigation is in the range of five to seven barn. The second type is a photodissociation process caused by an energetic photon emitted from a larger distance by one of the nuclei. It induces nuclear reactions in the other nucleus on impact. The cross section of this photodissociation process depends crucially on the type of the colliding ions. One finds cross sections of roughly 85 barn for RHIC in the Au mode, 200 barn for LHC in the Pb mode and 3

barn for LHC in the Ca mode [19]. In the following we list the approximate luminosities per bunch crossing \mathcal{L}_b and the corresponding probability of hadronic events per bunch crossing $\mathcal{P}_h = \sigma_h \mathcal{L}_b$, where the hadronic cross section σ_h is a combination of the purely hadronic and the photo-dissociation cross section. We obtain

$$\mathcal{L}_b = \begin{cases} 2.2 \times 10^{19} \text{ cm}^{-2}, \\ 3.75 \times 10^{20} \text{ cm}^{-2}, \\ 10^{23} \text{ cm}^{-2}, \end{cases} \quad \mathcal{P}_h \approx \begin{cases} 0.004 \text{ for RHIC, Au mode,} \\ 0.075 \text{ for LHC, Pb mode,} \\ 1 \text{ for LHC, Ca mode.} \end{cases}$$

By virtue of this figures we may conclude, that for Au and Pb the hadronic event rates are small enough to see DM-production in anticoincidences with the production of additional hadrons. In contrast this seems to be quite an impossible task for the Ca mode at LHC.

A second, significant source of background for the decay of the OM is caused by the production of free e^+e^- pairs by the two nuclei. In order to estimate this effect, we consider the e^+e^- pair production via the standard two-photon mechanism. The cross section of this process, σ_e , is estimated with the well-known Racah-formula (see [16] for details). We obtain $\sigma_e \approx 35\,000$ barn for RHIC and $\sigma_e \approx 225\,000$ barn for LHC. This is orders of magnitudes larger than the production cross section for the DM. A remedy for this problem might be a precise determination of the invariant mass of the electron-positron pair. The production cross section for an e^+e^- pair having an invariant mass near $2m_\mu$ with mass spread Δm is calculated using Eq. (5) with the replacement of $\sigma_{\gamma\gamma}$ by the cross section for the process $\gamma\gamma \rightarrow e^+e^-$:

$$\Delta\sigma(A_1 A_2 \rightarrow A_1 A_2 e^+ e^-) = \frac{(Z\alpha)^4}{\pi m_\mu^2} G(\delta) \left(\ln \frac{4m_\mu^2}{m_e^2} - 1 \right) \frac{\Delta m}{m_\mu} \approx 1.8 \times 10^7 \frac{\Delta m}{m_\mu} \sigma_{\text{PM}}. \quad (40)$$

Because the orthodimuonium production rate is comparably low, even a realistic mass resolution of 1 MeV would not fit our goal to distinguish the background from the signal of the orthodimuonia. Hence, it seems to be a very difficult task to observe the orthostate of dimuonium in heavy ion collisions.

This situation is different for the parastate. The main non-hadronic background to the the decay of the PM atoms is the two photon production process $A_1 A_2 \rightarrow A_1 A_2 + \gamma\gamma$. It can be described as the radiation of two (virtual) photons and subsequent light by light scattering (via an electronic loop). The cross section for this process is given by Eq. (5) with the replacement of $\sigma_{\gamma\gamma}$ by the cross section of light by light scattering. It is five orders less than σ_e and for invariant masses > 200 MeV of the photon pair it drops by five more orders. Nevertheless, the total free photon pair production cross section for all energies greater than 200 MeV is still larger than the production cross section for PM by a factor of $\approx \alpha^{-1}$. To improve the situation one might again try to fix the invariant mass m as precisely as possible. In general, a relative precision $\Delta m/m$ at $m^2 \approx 4m_\mu^2$ will lead to a signal-to-noise ratio of the order of $\alpha^{-1} \Delta m/m$.

$$\Delta\sigma(A_1 A_2 \rightarrow A_1 A_2 \gamma\gamma) = 0.95 \frac{Z^4 \alpha^6}{2 m_\mu^2} G(\delta) \frac{\Delta m}{m_\mu} \approx \frac{1}{\alpha} \frac{\Delta m}{m_\mu} \sigma_{\text{PM}}. \quad (41)$$

So the signal to background ratio becomes about 0.75 for mass resolution $\Delta m = 1$ MeV. This corresponds to a determination of the invariant mass of the decay products of PM with

a precision of roughly 5×10^{-3} . By contrast, for OM, a determination of the invariant mass of the electron-positron pair to an accuracy of the order of 10^{-7} would be necessary in order to reach a comparable signal-to-noise ratio.

Another possibility to further improve the situation is to take into account only highly relativistic dimuonium systems, which decay outside the nuclear collision region. The electron-positron or photon pair (for OM and PM, respectively) is produced outside the interaction region. DM atoms decay after travelling a typical decay length is $\ell \approx \varepsilon/(2m_\mu)c\tau$ (see Table II). This distance is increased for the excited dimuonia. The opportunity to observe excited dimuonium states in this approach will be better than that for the ground state despite the smaller production rate. The task left in this picture is to reconstruct the vertices of the decays, which necessitates a vertex detector.

V. RESULTS AND DISCUSSION

We have analyzed the production of bound states consisting of a muon and an antimuon in relativistic heavy ion collisions. The analysis of the parastate production was performed for the dominating two photon process. The two photon approximation describes the production of the parastate with an accuracy of $(1 \div 2)\%$. A novel three photon mechanism for the production of the orthostates was developed. The accuracy of this approximation is $(6 \div 12)\%$. The theoretical uncertainty of our results is primarily due to multiphoton processes. Other sources of uncertainty like the dependence on the nuclear form factor or corrections to the equivalent photon spectrum, have been analyzed in detail. They are on the level of one percent. Because multiphoton processes enhance the production rate, our results should be regarded as a lower bound on the total production.

We obtained numerical results for the dimuonium production at the new heavy ion colliders RHIC and LHC. The results for all colliders and for a set of atomic states are presented in Table II. In Table II we also consider the properties of the atomic 2P dimuonic state which is produced in atomic transitions from 3S and 4S¹.

The dimuonic atoms travel, after production, with small angular spread along the beam axis. Therefore they are detectable by their decay products only. In general the extraction of a signal from the experiment will be easier for paradimuonium than for orthodimuonium. The reasons are twofold,

- the total production cross section is much larger and
- the background is significantly reduced.

As it has been shown in Sec. IV, the photon pair background shadowing the paradimuonium signal is roughly five orders of magnitude smaller than the free electron-positron pair background shadowing the signal from orthodimuonium. Additionally, the total production

¹The results are obtained according to the treatment of recoil effects in Ref. [26]. The atomic transitions in heavy fermionium has been discussed in Ref. [27]. The DM spectrum is considered in detail in Ref. [2].

cross sections for para states are larger than those for ortho states by a factor of 10 to 100, depending on the collider and the nucleus used (see Table II). We expect a favourable signal-to-noise ratio for the parastate if the energy of the photon pair can be determined with a precision of roughly 1 MeV.

ACKNOWLEDGEMENTS

I. F. G., S. K. and V. G. S. are grateful to the Max-Planck-Institut für Physik komplexer Systeme for warm hospitality. U. D. J. wishes to thank DAAD for continued support. This work was supported in part by the grants INTAS-93-1180ext and the grant RFBR 96-02-19079 from the Russian Foundation for Basic Research. The work of U. D. J., F. K. and G. S. was additionally supported by GSI (Darmstadt), BMBF and DFG. D. Ivanov, V. Ivanov, K. Melnikov and G. Baur are gratefully acknowledged for stimulating discussions.

APPENDIX A: PARADIMUONIUM LIFETIME

We consider briefly the lifetime of the parastates of dimuonium. Because of the higher production rate of parastates, this is of interest in the context of possible experiments. The leading term is caused by the $\gamma\gamma$ decay,

$$\Gamma^{(0)}(n^1S_0) = \frac{\alpha^5 m_\mu}{2 n^3}. \quad (\text{A1})$$

Typical contributions to the next-to-leading order (NLO) corrections are depicted diagrammatically in Fig. 6. The corrections are evaluated in [2] as

$$\Delta\Gamma^{\text{NLO}}(1^1S_0) = 4.79 \frac{\alpha}{\pi} \Gamma^{(0)}(1^1S_0) \quad (\text{A2})$$

and

$$\Delta\Gamma^{\text{NLO}}(2^1S_0) = 4.65 \frac{\alpha}{\pi} \Gamma^{(0)}(2^1S_0). \quad (\text{A3})$$

The next-to-next-to-leading order (NNLO) corrections include the large logarithmic factors $\ln(1/\alpha)$ and $\ln^2(m_\mu/m_e)$. We consider here these logarithmic terms. The $\ln(1/\alpha)$ term is of the same form as for parapositronium [28],

$$\Delta\Gamma_1^{\text{NNLO}}(n^1S_0) = 2 \alpha^2 \ln\left(\frac{1}{\alpha}\right) \Gamma^{(0)}(n^1S_0). \quad (\text{A4})$$

The double mass ratio logarithm does not have an analogy in parapositronium. The relevant Feynman diagrams are depicted in Fig. 7. We obtain the result,

$$\Delta\Gamma_2^{\text{NNLO}}(n^1S_0) = (1+2) \frac{4 \alpha^2}{9 \pi^2} \ln^2\left(\frac{m_\mu}{m_e}\right) \Gamma^{(0)}(n^1S_0). \quad (\text{A5})$$

The terms $(1+2)$ originate from the diagrams in Fig. 7a and Fig. 7b, respectively. The calculation of the double logarithmic corrections is done here by the evaluation of the imaginary part of the diagrams in Fig. 7. The real part of these diagrams contributes to the hyperfine structure in higher order. The final results for the lifetimes are $\tau(1^1S_0) = 0.59504(22) \times 10^{-12}$ s and $\tau(2^1S_0) = 4.7619(17) \times 10^{-12}$ s.

APPENDIX B: DEPENDENCE OF THE ORTHOSTATE PRODUCTION ON THE FORM FACTOR

Employing the approximate form factor given in Eq. (7), we evaluate the integral Eq. (31) analytically. First we observe that the predominant contribution to B is caused by the region where $p_{\perp}^2/\Lambda^2 < 1$. In this region $\tau = p_{\perp}^2/(4m_{\mu}^2) < 0.1$. Therefore we may put $\tau = 0$ in Eq. (29). We integrate

$$\Phi(\Lambda^2 u) = \frac{1}{\pi} \int \frac{(\mathbf{r}^2 - 1)}{(\mathbf{r} - \mathbf{n})^2(\mathbf{r} + \mathbf{n})^2} \frac{d^2 r}{[1 + (u/4)(\mathbf{r} - \mathbf{n})^2][1 + (u/4)(\mathbf{r} + \mathbf{n})^2]}. \quad (\text{B1})$$

The relation

$$\mathbf{r}^2 - 1 = \frac{1}{2} [(\mathbf{r} + \mathbf{n})^2 + (\mathbf{r} - \mathbf{n})^2 - 4]$$

proves to be useful for a simplification of the integrand. We can present the integral in Eq. (B1) in the form

$$\Phi(\Lambda^2 u) = -(2 + a_1) I_{11} - 2 I_{22} + (4 + a_1) I_{12}. \quad (\text{B2})$$

The integrals I_{ij} are defined as

$$I_{ij} = \frac{1}{\pi} \int \frac{d^2 r}{[(\mathbf{r} + \mathbf{n})^2 + a_i][(\mathbf{r} - \mathbf{n})^2 + a_j]},$$

where $a_1 = 4/u$. The auxiliary parameter $a_2 = \epsilon \rightarrow 0$ is introduced in order to regularize divergences in intermediate calculations. For the integrals I_{ij} we obtain after elementary integration

$$I_{11} = \frac{1}{\sqrt{1 + a_1}} \ln \frac{1 + \sqrt{1 + a_1}}{\sqrt{a_1}}, \quad I_{22} = \frac{1}{2} \ln \frac{4}{\epsilon}, \quad I_{12} = \frac{1}{4 + a_1} \ln \frac{(4 + a_1)^2}{a_1 \epsilon}.$$

Substituting these expressions into Eq. (B2) we obtain the result

$$\Phi(\Lambda^2 u) = \ln \frac{(1 + u)^2}{u} - \frac{4 + 2u}{\sqrt{4u + u^2}} \ln \frac{\sqrt{4 + u} + \sqrt{u}}{2}, \quad (\text{B3})$$

in which the dependence on the auxiliary parameter ϵ vanishes. Using this method we obtain a result of $B = 0.93$ in contrast to $B = 0.85$ with the exact form factor (cf. Eq. (33)).

REFERENCES

- [1] S. Karshenboim, U. Jentschura, V. Ivanov, and G. Soff, Phys. Lett. **B424**, 397 (1998).
- [2] U. Jentschura, G. Soff, V. Ivanov and S. Karshenboim, Phys. Rev. A **56**, 4483 (1997); S. Karshenboim, V. Ivanov, U. Jentschura, G. Soff, Zh. Eksp. Teor. Fiz. **113**, 409 (1998) (in Russian), JETP **86**, 226 (1998).
- [3] L. Nemenov, Yad. Fiz. **15**, 1047 (1972) (in Russian), Sov. J. Nucl. Phys. **15**, 582 (1972).
- [4] J. Malenfant in *AIP Conf. Proc.* **150** (Ed. F. Geesaman), p. 595, AIP, New York (1986), and J. Malenfant, Phys. Rev. D **36**, 863 (1987).
- [5] S. Bilen'kii, N. van Hieu, L. Nemenov and F. Tkebuchava, Yad. Fiz. **10**, 812 (1969) (in Russian), Sov. J. Nucl. Phys. **10**, 469 (1969).
- [6] G. A. Kozlov, Phys. At. Nucl. **48**, 167 (1988).
- [7] E. Holvik and H. A. Olsen, Phys. Rev. D **35**, 2124 (1987).
- [8] R. M. Barnett *et al.*, Phys. Rev. D **54**, 1 (1996).
- [9] S. Peggs (RHIC), *private communication*.
- [10] D. Brandt, K. Eggert, and A. Morsch, LHC Note 264, CERN AT 94-05 (DI).
- [11] C. T. Mungler, S. J. Brodsky and I. Schmidt, Phys. Rev. D **49**, 3228 (1994).
- [12] G. Baur *et al.*, Phys. Lett. **B368**, 251 (1996).
- [13] L. G. Afanasyev, A. S. Chvyrov, O. E. Gorchakov, M. A. Ivanov, V. V. Karpukhin, A. V. Kolomyichenko, V. I. Komarov, V. V. Kruglov, A. V. Kuptsov, L. L. Nemenov, M. V. Nikitin, Zh. P. Pustyl'nik, A. V. Kulikov, S. V. Trusov, V. V. Yazkov, G. G. Mkrtchya, and A. P. Kurov, Phys. Lett. **B308**, 200 (1993); L. G. Afanasyev, A. S. Chvyrov, O. E. Gorchakov, V. V. Karpukhin, A. V. Kolomyichenko, V. I. Komarov, V. V. Kruglov, A. V. Kuptsov, L. L. Nemenov, M. V. Nikitin, Zh. P. Pustyl'nik, A. V. Kulikov, S. V. Trusov and V. V. Yazkov, Phys. Lett. **B338**, 478 (1994).
- [14] R. Coombes, R. Flexer, A. Hall, R. Kennelly, J. Kirkby, R. Piccioni, D. Porat, M. Schwartz, R. Spitzer, J. Toraskar, S. Wiesner, B. Budnick and J. W. Kats, Phys. Rev. Lett. **37**, 249 (1976).
- [15] S. H. Aronson, R. H. Bernstein, G. J. Bock, R. D. Cousins, Jr., J. F. Greenhalgh, D. Hedin, M. Schwartz, T. K. Shea, G. B. Thomson and B. Winstein, Phys. Rev. Lett. **48**, 1078 (1982); S. H. Aronson, R. H. Bernstein, G. J. Bock, R. D. Cousins, Jr., J. F. Greenhalgh, D. Hedin, M. Schwartz, T. K. Shea, G. B. Thomson and B. Winstein, Phys. Rev. D **33**, 3180 (1986).
- [16] V.M. Budnev, I.F. Ginzburg, G.V. Meledin, V.G. Serbo, Phys. Rep. **C 15** 181, (1975).
- [17] Y. Tsai, Rev. Mod. Phys. **46** 815, (1974).
- [18] V.B. Berestetskii, E.M. Lifshitz, and L.P. Pitaevskii, Quantum Electrodynamics (Pergamon Press, 1982).
- [19] F. Krauss, M. Greiner and G. Soff, Prog. Part. Nucl. Phys. **39**, 503 (1997).
- [20] G. V. Meledin, V. G. Serbo, and A. K. Slivkov, Pis'ma v ZhETF **13**, 98 (1971) (in Russian); JETP Lett. **13**, 68 (1971).
- [21] L. N. Lipatov, and G. V. Frolov, Yad. Fiz. **13**, (1971) 588.
- [22] H. Cheng, and T. T. Wu, Phys. Rev. D **1**, 3414 (1970).
- [23] I. F. Ginzburg, S. L. Panfil, and V. G. Serbo, Nuclear Physics **B 284**, 685 (1987).
- [24] I. F. Ginzburg, S. L. Panfil, and V. G. Serbo, Nuclear Physics **B 296**, 569 (1988).
- [25] A. Bohr and B. R. Mottelson, Phys. Lett. **B100**, 10 (1981).
- [26] Z. Fried and A. D. Martin, Nuovo Cim. **29**, 574 (1963).

- [27] J. Moffat, Phys. Rev. Lett. **35**, 1605 (1975).
[28] I. B. Khriplovich and A. S. Yelkhovsky, Phys. Lett. **B246**, 520 (1990).

TABLES

Collider	Nucleus	Nuclear charge (Z)	Luminosity \mathcal{L} [$\text{cm}^{-2}\text{s}^{-1}$]	Lorentz factor (γ)	Bunch length [cm]
RHIC	AuAu	79	2×10^{26}	108	12
LHC	PbPb	82	3×10^{27}	2980	7.5
LHC	CaCa	20	4×10^{30}	3750	7.5

TABLE I. Experimental parameters of RHIC and LHC which must be taken into account for the production of dimuonium. The bunch length of 7.5 cm for the CaCa-channel at LHC is an estimate.

ATOMIC STATE PROPERTIES					ESTIMATED PRODUCTION PER YEAR		
Atom	State	J^{PC}	$c\tau$ [cm]	Decay mode	RHIC Au–Au	LHC Pb–Pb	LHC Ca–Ca
PM	1^1S_0	0^{-+}	0.0178	$\gamma\gamma$	310	40000	260000
PM	2^1S_0	0^{-+}	0.143	$\gamma\gamma$	40	5000	33000
PM	3^1S_0	0^{-+}	0.483	$\gamma\gamma$	12	1500	9800
PM	4^1S_0	0^{-+}	1.14	$\gamma\gamma$	5	630	4100
PM	8^1S_0	0^{-+}	9	$\gamma\gamma$	–	79	520
PM	10^1S_0	0^{-+}	18	$\gamma\gamma$	–	40	260
OM	1^3S_1	1^{--}	0.0538	e^+e^-	43	2700	2800
OM	2^3S_1	1^{--}	0.430	e^+e^-	5	330	340
OM	3^3S_1	1^{--}	1.45	e^+e^-	2	100	100
PM	2^1P_1	1^{+-}	0.462	$1^1S_0 \gamma$	–	60	400

TABLE II. Main properties of atomic states of dimuonium and their estimated production at LHC and RHIC per year (running time per year in our calculation is 10^7 s). The *decay mode* given here is the dominant mode which is most important for the detection.

FIGURES

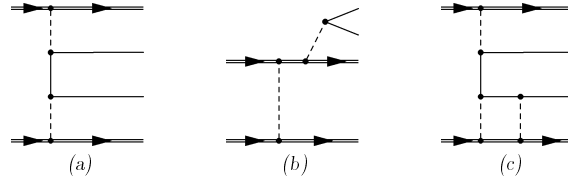


FIG. 1. Diagrams for two and three photon production mechanisms of fermion pairs in relativistic heavy ion collisions. In the case of dimuonium, the fermion pair is produced in a bound state.

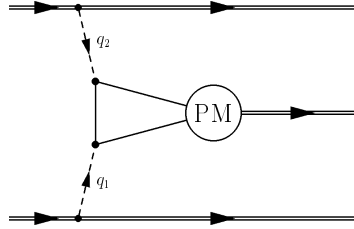


FIG. 2. Two photon production of paradimuonium by relativistic heavy nuclei.

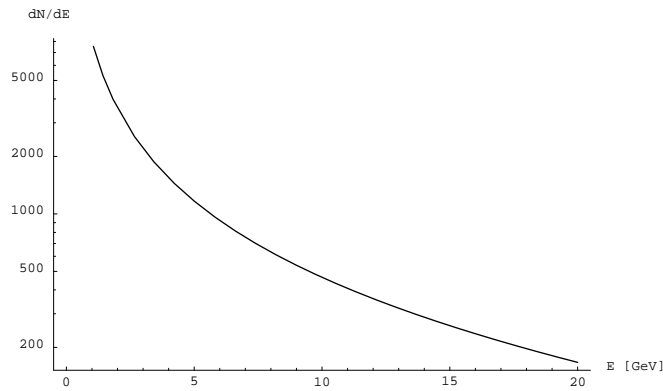


FIG. 3. Distribution of paradimuonium produced at LHC in the Pb mode over the energy (in GeV). The distribution is normalized to the annual production rate of 40 000 particles. The median of the distribution is at 1.12 GeV.

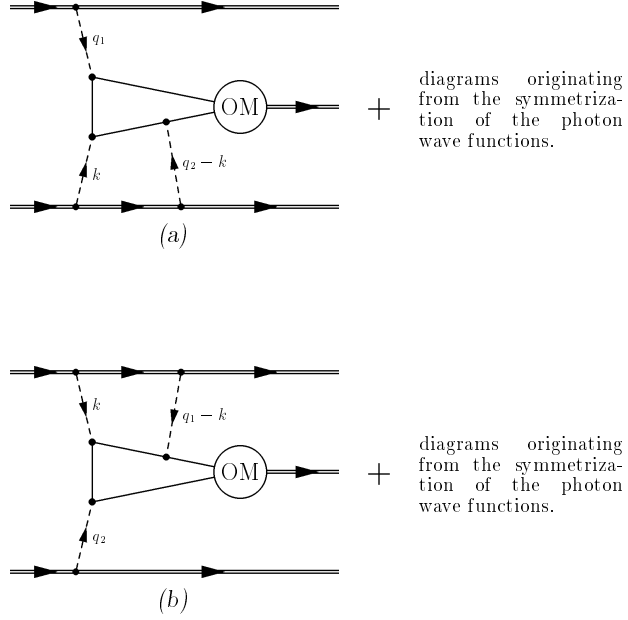


FIG. 4. Orthodimuonium production by a three photon fusion process.

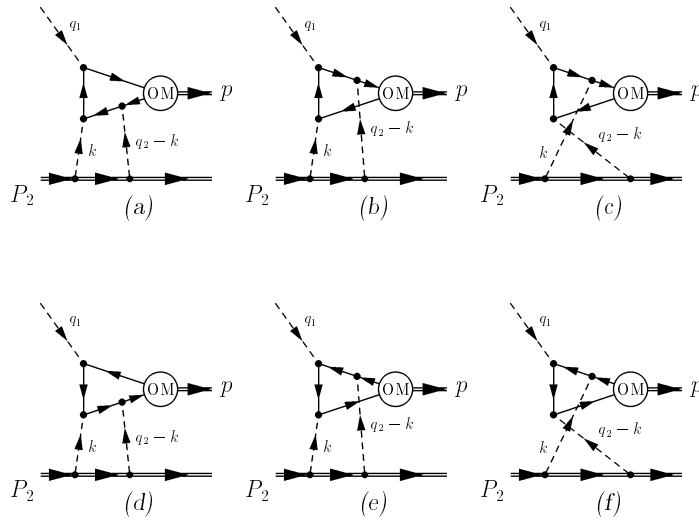


FIG. 5. Orthodimuonium production by a three photon fusion process. P_2 denotes the nuclear momentum, p is the momentum of the dimuonium system.

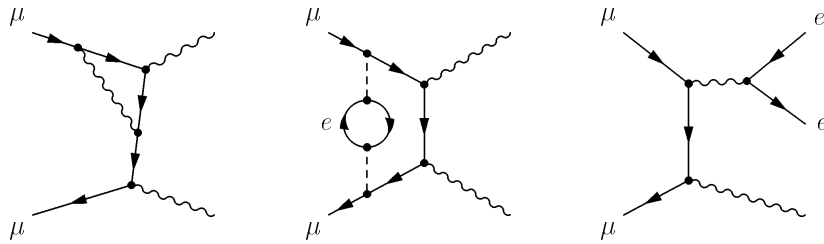


FIG. 6. Typical NLO corrections to the PM decay rate.

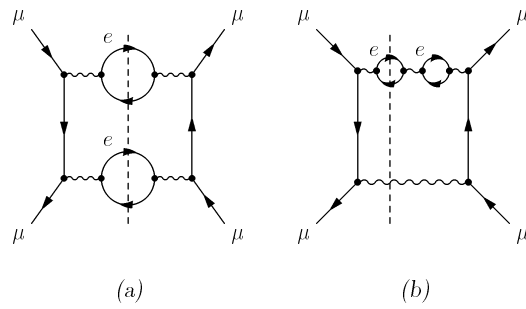


FIG. 7. Feynman diagrams for the double logarithmic NNLO corrections to the PM decay rate.